Pergamon

PII: S0301-9322(96)00057-2

Int. J. Multiphase Flow Vol. 23, No. 1, pp. 81–92, 1997

0301-9322/97 $17.00 + 0.00

ON THE EFFECTIVE PERMEABILITY OF SQUARE ARRAYS OF PERMEABLE FIBER TOWS

T. D. PAPATHANASIOU

Department of Chemical Engineering and Centre for Composite Materials, Imperial College of Science, Technology and Medicine, London SW7, U.K.

(Received 8 January 1996; in revised form 3 July 1996)

Abstract—This paper presents a computational investigation on the influence of the meso- (inter-tow; ϕ_i) and micro-scale (intra-tow; ϕ_t) porosities on the effective transverse permeability (K_p) of square arrays of permeable fiber tows. The equations governing Stokes flow are solved, using the Boundary Element Method, in unit cells which consist of a number of fiber-like filaments, arranged in square packing within the circular perimeter of the tow. The key finding of this study is that the permeability ratio (K_p/K_s), where (K_s) is the permeability of the corresponding square array of impermeable tows, can be described as a power-law function of the effective intra-tow porosity (χ). Based on this, a scaling is proposed according to which the computational results for K_p at relatively low values of the inter-tow porosity ($0.25 < \phi_i < 0.5$) collapse on a power-law curve with exponent 2.1 when plotted against (χ). Copyright © 1996 Elsevier Science Ltd.

Key Words: permeability, resin transfer molding, Stokes flow, porous media, boundary element method

1. INTRODUCTION

Recent years have seen significant advances in the theoretical description of flow of polymeric resins (Pillai *et al.* 1993; Skartsis *et al.* 1992) or molten metals (Nagelhout *et al.* 1995) through fibrous porous media. Today it is possible to predict the essential characteristics of the filling of a mold containing a fiber preform using computer-aided design models such as the LIMS package (Bruschke and Advani 1993a). This and other similar models for resin flow in fiber preforms are based on Darcy's law for flow in porous media (Darcy 1856), according to which the local volume-averaged fluid velocity is proportional to the local pressure gradient. The constant of proportionality is the *permeability* of the porous medium. Even though Darcy's model is a robust and well-accepted description of flow in porous media (Parnas and Phelan 1991), its success in simulating flow in fiber preforms depends critically on the quality of available data for the permeability and, most importantly, its variation throughout the preform. A significant amount of research has been devoted to deriving predictive models for the permeability of systems consisting of uniform, aligned cylinders (Sangani and Acrivos 1982; Drummond and Tahir 1984; Gebart 1992; Bruschke and Advain 1993b). Such models are usually in good agreement with experimental data for flow of Newtonian and shear-thinning fluids across experimental beds of aligned fibers, as well as with numerical calculations for flow of Newtonian and shear-thinning fluids across unit cells representing similar systems. Refinements to include the effect of perturbations in fiber size and spacing have more recently been introduced (Lundstrom and Gebart 1995).

The significant progress outlined above notwithstanding, difficulties still remain in predicting, reliably, the flow patterns during resin impregnation of a fiber preform. The main reason for this is the simple fact that a fiber preform is never a bed of uniform, aligned fibers. Heterogeneities exist, either as a (deliberate or accidental) result of the preform fabrication process or as a consequence of the filling process itself. Such heterogeneities range from through-thickness variations in structure, to the presence of air pockets within fiber tows due to poor resin impregnation (Pillai *et al.* 1993; Pillai and Advani 1995) to the compaction of the preform at elevated filling rates (Gutowski *et al.* 1987; Skartsis *et al.* 1992; Lam and Kardos 1991). It is now clear in the composites literature (Parnas and Phelan 1991; Pillai *et al.* 1993; Pillai and Advani 1995; Sadiq *et al.* 1995; Summerscales 1993) that an important source of flow irregularities, such as flow

fingering, the dependence of permeability on flowrate or on the degree of bed saturation and the formation of voids during preform impregnation, is the wide difference in pore size between the inter- and the intra-tow regions. It is evident that under a pressure gradient, resin will flow through both, the inter- and the intra-tow space, each of which will contribute to the overall flow resistance of the medium. Three distinct length scales must therefore be considered in a realistic model for flow through fiber preforms (Lundstrom and Gebart 1995; Pillai and Advani 1995): A *macro-scale* (related to the leading dimension of the composite part), a *meso-scale* (related to the size of bundles of fibers (tows) comprising the preform) and a *micro-scale* (associated with the size of the individual filaments comprising each tow). Two porosities can thus be distinguished: a meso-scale porosity (or, inter-tow porosity, (ϕ_i)), defined as the voidage between fiber tows in the preform, and a micro-scale porosity (or, intra-tow porosity, (ϕ_t)), defined as the voidage between individual filaments inside a tow.

From the preceding discussion it becomes clear that treating fiber tows as impermeable entities is, in principle, incorrect. It has indeed been shown (Sadiq *et al.* 1995) that, when individual fibers are replaced with fiber bundles of equal total diameter in a test fiber-bed, the measured permeabilities are not in agreement with the predictions of existing theoretical models. The effective permeability of the new assembly was found to be closer to the permeability of systems comprised of solid, impermeable tows than to the permeability of systems consisting of uniformly distributed fibers with diameter equal to that of the filaments in each tow at the same overall volume fraction. Sadiq *et al.* (1995) have also shown that neither the global fiber volume fraction nor the fiber volume fraction inside the tow are suitable parameters to be used in existing theoretical models to calculate (K_p). Instead, they proposed that correlations of the form

$$\frac{K_p}{K_s} = 1 + k_1\chi + k_2\chi^2 + k_3\chi^3 + \cdots \qquad [1]$$

should be used in relating the permeability ratio (K_p/K_s) to the effective intra-tow porosity (χ) (defined as $\chi = 1 - (1 - \phi_t)/(1 - \phi_{max})$). In [1] ($K_s$) is the permeability of an array of impermeable cylinders of the same size as the fiber tows and use of (χ) is consistent with scalings adopted in previous analyses of flow through particle clusters (Lewis and Nielsen 1970; Phan-Thien *et al.* 1991).

In spite of the growing realisation of the importance of the inter- and intra-tow length scales, only limited results (theoretical or experimental) exist in quantifying the effect of the interplay between meso- and micro-scale porosities on the permeability of a fiber preform. Based on geometrical arguments, Summerscales (1993) proposed a procedure to determine the effect of fiber clustering on permeability through the use of a modified hydraulic radius. The predictions of this model are in qualitative agreement with the experimental observation that fiber clustering results in an enhanced resin flow compared to a uniform distribution of the same number of fibers. Parnas and Phelan (1991) addressed the problem of the coupling of the flow of resin through the voids separating fiber tows with the microscopic flow associated with the impregnation of individual tows, by considering the latter as flow sinks which remove fluid from the main (macroscopic) flow as the resin fills a dry preform. In qualitative agreement with experimental observations, their model predicts that the two competing flow processes result in an effective permeability which is higher in dry preforms than in saturated ones. Pillai *et al.* (1993) and Pillai and Advani (1995) recognised explicitly the importance of multiple length scales on the effective permeability of a fiber-tow assembly. They considered Stokes' flow in the inter-tow space, treated the intra-tow region as a porous medium with an effective permeability (κ) and took into account the presence of pockets of air trapped within fiber tows. The difficulty associated with matching the boundary conditions for the two problems at the tow-fluid interface was bypassed by replacing Darcy's model in the intra-tow region with Brinkman's equation. Pillai and Advani developed an analytical model for the effective permeability of this system based on lubrication theory and compared its predictions to those of the CFD package FIDAP. Even though the predictions of this model were in qualitative agreement with experimental evidence, they were found sensitive to the value of the effective intra-tow permeability (κ). Quantitative agreement between model predictions and experiment could not be obtained when κ was calculated from existing models (e.g. Gebart 1992 or Bruschke and Advani 1993b) and a heuristic approach to obtain better estimates for κ was suggested by

Pillai *et al.* (1993). Along the same lines, Phelan and Wise (1996) developed a semi-analytical model for the effective permeability of arrays of fiber tows with elliptical crossection. The predictions of their model were in good agreement with finite element results using the CFD package FIDAP and in reasonable agreement with the experimental data of Sadiq *et al.* (1995). The main difficulty in this approach lies in assigning physically realistic values to the intra-tow permeability and in the use of the Brinkman equation to describe the flow inside fiber tows. The suitability of the latter in modelling viscous flow near the surface of a porous medium has been questioned by Larson and Higdon (1986, 1987), who have carried out extensive computations for Stokes flow past a semi-infinite lattice of cylindrical inclusions. These computations indicated that flow over the surface of such a porous medium is inherently a surface phenomenon, with an extremely rapid decay of velocities even at low concentrations of the particulate phase, and that attempts to describe it in terms of averaged quantities will miss important details. Further development of such models will definitely benefit from more extensive experimentation and, hopefully, from comparisons with the results of micromechanical computations such as those presented in this study. A more detailed comparison between computations similar to those presented in the present study and the results of the model proposed by Phelan and Wise (1996) is currently under way.

The objective of the present communication is to further quantify the effect of the inter- and intra-tow porosities on the apparent transverse permeability of arrays of permeable fiber tows and to suggest appropriate scalings. In a manner similar to previous investigations using the BEM in multi-particle systems (Larson and Higdon 1986, 1987; Papathanasiou 1996) the equations governing Stokes' flow are solved in the entire region occupied by the fluid in both the inter- and intra-tow regions. Microstructural characteristics of the tow are therefore directly reflected in the thus determined effective permeabilities and furthermore, assumptions about the physics of the flow at the fluid-tow interface are avoided. These are considered the main strengths of the present methodology. A large number of simulations is performed for a range of inter- and intra-tow porosities; based on these results we propose models for the effective permeability in which the influence of (ϕ_t) and (ϕ_i) is explicitly included. It should be pointed out that since the fluid is considered to occupy the entire inter-filament space, our results correspond to the permeability of fully-saturated systems.

2. THE MATHEMATICAL MODEL

The flow transverse to an assembly of permeable fiber tows (including flow in the inter- and intra-tow regions) is modelled as linear, incompressible and inertialess. In the absence of body forces, the equations governing such flow in a general multi-connected domain (Ω) can be written as (Pozrikidis 1992; Ladyzhenskaya 1963):

$$\frac{\partial^2 u_i(\mathbf{x})}{\partial x_j \partial x_i} = \frac{\partial P(\mathbf{x})}{\partial x_i} \quad x \in \Omega \quad \text{(momentum)} \tag{2}$$

$$\frac{\partial u_i(\mathbf{x})}{\partial x_i} = 0 \quad x \in \Omega \quad \text{(continuity)} \tag{3}$$

where $\mathbf{u}$ and $\mathbf{x}$ are the velocity and location vectors, respectively. The components of the traction vector $\mathbf{t}$, needed in the boundary integral formulation of the Stokes' problem, are obtained from the total stress tensor ($\mathbf{T}$) as:

$$t_i = \sum_{j=1}^{ND} T_{ij} n_j \tag{4}$$

where $ND = 2$ for two- and $ND = 3$ for three-dimensional problems, respectively, and $\mathbf{n}$ is the local vector normal to the boundary.

2.1. The Boundary Element Method

The application of the BEM in the solution of Stokes flow problems in complex, multiply-connected domains is well-documented (Phan-Thien *et al.* 1991; Ingber and Li 1991; Pozrikidis 1992; Brebbia and Dominguez 1992). Briefly, in the BEM the original Stokes problem

is recast in an integral form by considering a weighted residual statement of the differential equations with weighting functions given by the fundamental solutions for velocity and tractions ($\mathbf{u}^*$, $\mathbf{t}^*$). The resulting Boundary Integral Equation (BIE) is:

$$c_{mn}(\xi)u_n(\xi) + \int_S t^*_{mn}(\xi, \mathbf{x})u_n(\mathbf{x})\mathrm{d}S = \int_S u^*_{mn}(\xi, \mathbf{x})t_n(\mathbf{x})\mathrm{d}S \qquad [5]$$

where ξ indicates a field point and the integrals are in the sense of Cauchy principal values. In two dimensions, the fundamental solution for the velocity and the associated solution for the tractions are given by:

$$u^*_n = u^*_{mn}e_m \quad \text{where} \quad u^*_{mn} = \frac{1}{4\pi}\cdot\left[\ln(|\mathbf{r}|^{-1})\delta_{mn} + \frac{r_n r_m}{|\mathbf{r}|^2}\right] \qquad [6]$$

and

$$t^*_n = t^*_{mn}e_m \quad \text{where} \quad t^*_{mn} = -\frac{1}{\pi}\frac{r_m r_n}{|\mathbf{r}|^3}\frac{\partial \mathbf{r}}{\partial \mathbf{n}}. \qquad [7]$$

$\mathbf{r}$ is the vector between ξ and $\mathbf{x}$, r_n and r_m indicate the projections of $\mathbf{r}$ in each of the principal directions of the global coordinate system and e_m indicates the unit vector in the direction m. The BIE is discretised by subdividing the domain boundary into boundary segments (elements) within which the velocities and tractions are given polynomial approximations with the use of Langrangian shape functions. Following numerical evaluation of the boundary integrals and introduction of the influence matrices ($\mathbf{H}$ and $\mathbf{G}$), the global system of equations can be written as:

$$[\mathbf{H}]\cdot\{\mathbf{u}\} = [\mathbf{G}]\cdot\{\mathbf{t}\}. \qquad [8]$$

This system is further rearranged by separating the parts of the $\mathbf{u}$ and $\mathbf{t}$ vectors known from the boundary conditions (Papathanasiou *et al.* 1994) and the resultant system of linear equations is solved for the unknown velocities and tractions on the boundaries of the computational domain. The velocities at points in the interior of the flow domain can be obtained from the solution at the boundary in a simple post-processing step using Somigliana's identity (Brebbia and Dominguez 1992).

3. RESULTS AND DISCUSSION

The effect of the microstructure on the transverse permeability (K_p) of arrays of permeable, multi-fiber tows of circular cross-section is investigated through numerical solution of the Stokes equations in unit cells of the type shown in figure 1 for various combinations of the inter- and the intra-tow porosities. The inter-tow porosity is defined as

$$\phi_i = 1 - \frac{R_t^2}{HL}\frac{\pi}{2},$$

where R_t is the radius of the tow and H and L are the length and height of the unit cell. The arrangement of the fibers inside the tow is in regular square array and each tow contains at least 60 fibers. It was determined (Papathanasiou 1996) that for $N_f > 60$, the predicted permeability was roughly independent of the number of fibers in the tow. The intra-tow porosity is defined as

$$\phi_t = 1 - N_f\left[\frac{R_f}{R_t}\right]^2,$$

where N_f is the number and R_f the radius of the (cylindrical) filaments in each tow. Following solution of the Stokes equations, K_p is determined through numerical integration of the computed outflow velocity profile. The boundary conditions used were with (reference to figure 1): symmetry

conditions along the top and bottom boundaries, fixed pressure drop between right and left boundaries and no-slip conditions on the surface of the fibers.

3.1. Flow distribution through the unit cell

Figure 1 shows typical multi-filament unit cells used in the computations of this study, along with numerically-computed trajectories of (massless) tracer particles placed at various locations along the left-hand (inlet) boundary of the unit cell. It is evident from the form of these trajectories that the flow "senses" the presence of the tow and re-distributes itself to take advantage of the low resistance region near the "top" symmetry line. Weak recirculation regions near the lower symmetry axis appear to persist even for intra-tow porosities as high as 70%. It is also seen that even at intra-tow porosities as high as 50% the tow behaves largely as an impermeable entity, with only a small part of the material flowing through the unit cell travelling through the tow itself. As the internal porosity increases further to 60 and 70%, progressively more of the tracer particles actually pass through the tow.

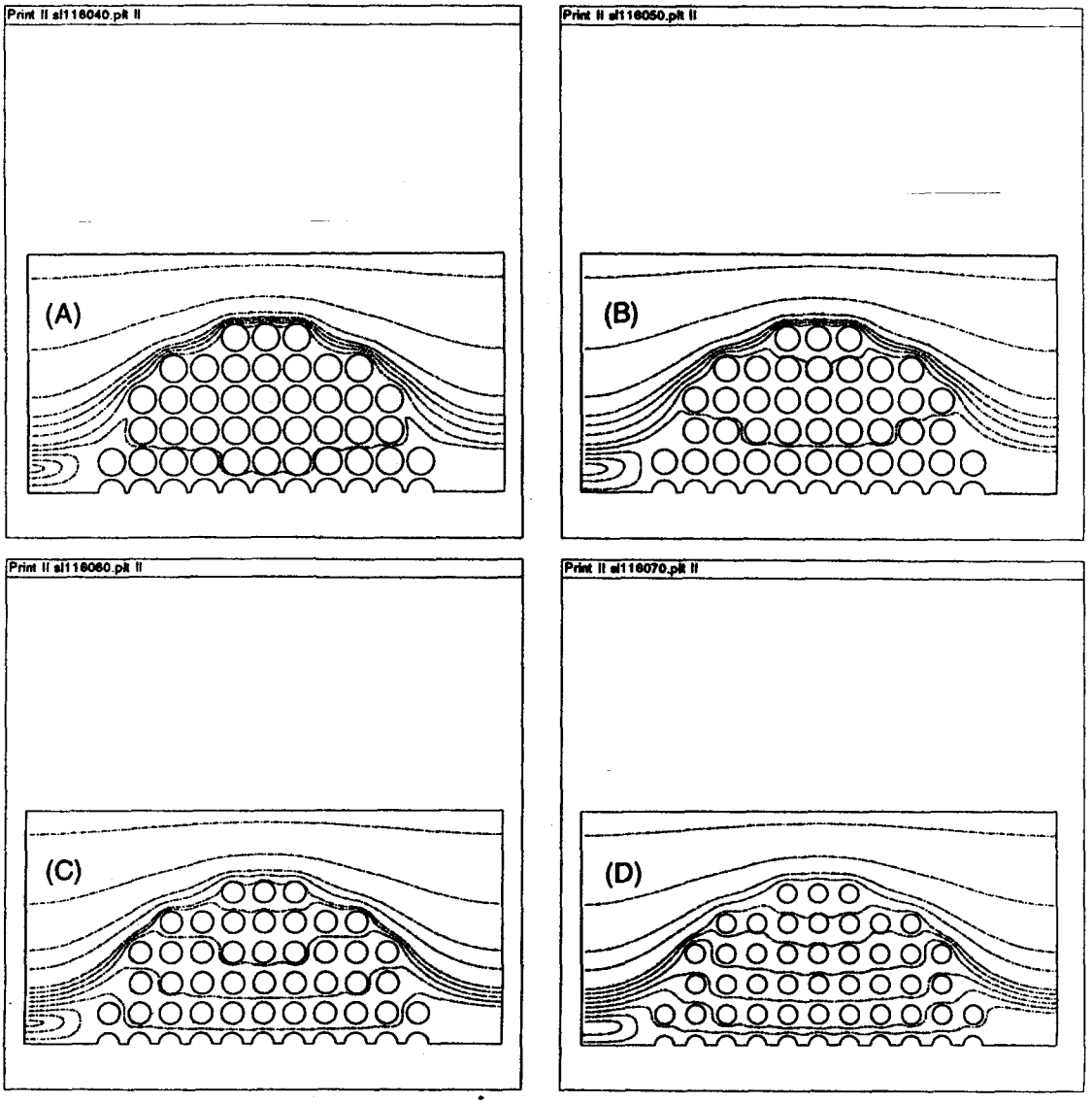

Figure 1. Typical multi-fiber unit cells used in the computations of the effective permeability of assemblies of permeable fiber tows, along with the trajectories of tracer particles. Conditions are (A): $\phi_i = 0.6$, $\phi_t = 0.4$; (B): $\phi_i = 0.6$, $\phi_t = 0.5$; (C): $\phi_i = 0.6$, $\phi_t = 0.6$; (D): $\phi_i = 0.6$, $\phi_t = 0.7$.

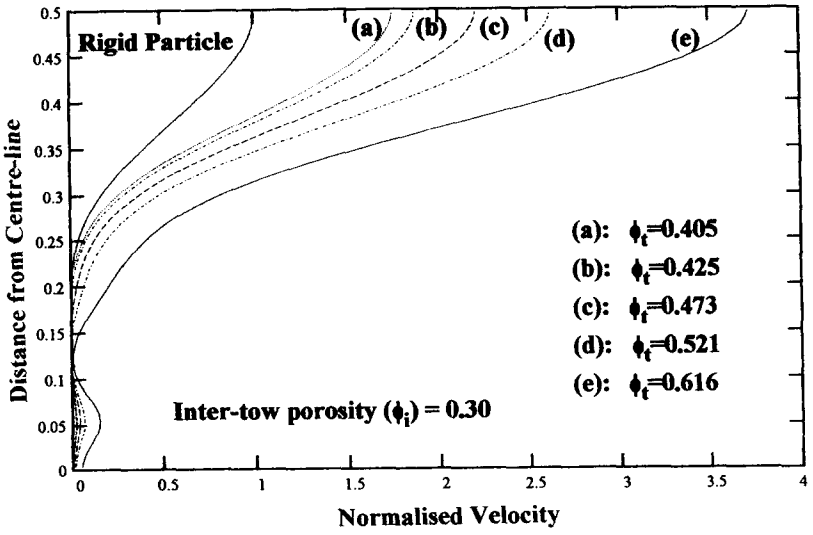

Figure 2. Velocity profiles along the right-hand vertical boundary of the unit cell (as shown in figure 1) corresponding to an inter-tow porosity of 0.3, at various levels of the intra-tow porosity. The result for an impermeable tow ("rigid particle") is shown as the solid line to the left. Velocities are normalised with respect to the maximum velocity corresponding to an impermeable tow.

The effect of the intra-tow porosity on the distribution of flow in the unit cell at lower values of the inter-tow porosity ($\phi_i = 0.3$) is further shown in figure 2, in which the velocity profile along the right-hand vertical boundary is plotted for values of the intra-tow porosity ranging from 0.405 to 0.616. The velocity profile corresponding to an impermeable tow is also shown for comparison. In figure 2 the computed velocities have been normalised by dividing with the maximum velocity corresponding to an impermeable tow. It is seen that as ϕ_t increases, the outflow velocity profiles become substantially and qualitatively different from the one corresponding to an impermeable tow. This is typical of unit cells with low porosity. It is also seen that as ϕ_t increases, progressively more fluid passes through the channel between the first two rows of intra-tow fibers (located at $y = 0.05$ on the vertical axis of figure 2.

3.2. *The effective permeability of the tow array*

The work of Sadiq *et al.* (1995) has indicated that the effective permeability of arrays of fiber bundles cannot be predicted by existing theoretical models (such as those of Gebart 1992 and Bruschke and Advani 1993b) which have been derived from unit-cells containing one impermeable fiber. It has been shown that K_p is closer to the permeability of a system comprised of solid, impermeable tows than to a system comprised of uniformly distributed fibers with diameter equal to that of the filaments in each tow at the same overall volume fraction. Sadiq *et al.* (1995) have also shown that neither the global fiber volume fraction nor the fiber volume fraction inside the tow are suitable parameters to be used in existing theoretical models to calculate K_p. These observations have been confirmed in the context of the present study. This result is not surprising, since it is known that the flow-resistance of a cluster of particles is larger than justified by the volume fraction of the particles alone; in particle clusters, the liquid in the neighbourhood of the particles is "immobilised" and contributes to an *effective* particle volume fraction which is greater than the actual volume fraction of the particles. This has been recognised in previous theoretical studies of flow in fibrous porous media (Gebart 1992; Gutowski *et al.* 1987) and consequently, the fiber volume fraction at maximum packing (ϕ_{max} or ϕ_m) has been included in the adopted scalings. The same approach was followed by Sadiq *et al.* (1995) in using [1] to interpret experimental data for the effective permeability of arrays of fiber bundles. Our objective here is to further quantify the influence of the meso- and micro-scale porosities of the unit cell on the effective permeability of the system by carrying out a number of detailed simulations in which the microstructure of the tow is carefully controlled. In these simulations the inter-tow porosity ϕ_i varied between 0.25 and 0.7 and the intra-tow porosity ϕ_t between 0.3 and 0.6.

Table 1. Results of the BEM computations in terms of the ratio K_p/K_s for a range of the inter- ϕ_i and the intra-tow ϕ_t porosities. The effective intra-tow porosity χ is defined as: $\chi = 1 - (1 - \phi_t)/(1 - \phi_{max})$. $\phi_{max} = 1 - \pi/4$

χ	$\phi_i = 0.25$	$\phi_i = 0.30$	$\phi_i = 0.35$	$\phi_i = 0.40$	$\phi_i = 0.50$	$\phi_i = 0.60$	$\phi_i = 0.70$
0.096	1.46	1.10	1.03	1.03	1.02	—	—
0.12	1.72	1.18	1.07	1.06	1.03	—	—
0.15	2.08	1.26	1.11	1.09	1.05	1.04	1.03
0.17	2.45	1.35	1.16	1.12	1.07	—	—
0.19	2.93	1.45	1.21	1.15	1.09	1.06	—
0.22	3.46	1.55	1.26	1.18	1.10	—	—
0.23	3.78	1.61	1.28	1.20	1.11	—	—
0.24	4.13	1.79	1.32	1.25	1.15	1.10	1.06
0.27	5.44	1.92	1.38	1.29	—	—	—
0.28	—	—	—	—	1.19	1.12	—
0.33	7.99	2.33	1.55	1.40	1.23	1.14	1.09
0.39	11.4	2.84	1.75	1.54	1.31	1.18	1.11
0.45	—	—	—	1.68	1.35	1.22	—
0.51	22.1	4.28	2.28	—	—	—	1.16
0.63	—	—	—	—	—	—	1.21

The results of the BEM computations are presented in table 1 in terms of the permeability ratio (K_p/K_s). The permeability of the corresponding array of impermeable cylinders (K_s) has been calculated separately through the BEM using meshes of size comparable to that used in the multi-fiber calculations. It is recognised that presentation of the results in terms of the ratio K_p/K_s may be problematic when the inter-tow porosity approaches maximum packing, at which point K_s drops sharply to zero (while K_p assumes a non-zero value). In the present study K_s is only used for ease of presentation and to facilitate comparisons; the value of K_p is the primary quantity calculated directly from the outflow velocity profile for each combination of ϕ_i and ϕ_t.

It can be seen from the data of table 1 that the relationship between K_p and χ is distinctively non-linear, especially at lower values of the inter-tow porosity ($\phi_i < 0.4$). Even in the case of higher ϕ_i, when a straight line can be "fitted" through the BEM results, as shown in figure 3, it is clear that the resultant least-squares lines have intercepts that deviate consistently from unity. The intercepts of the least-squares fits between K_p/K_s and χ corresponding to $\phi_i = \{0.4, 0.5, 0.6, 0.7\}$ are $\{0.814, 0.904, 0.949, 0.968\}$, respectively. This is of course unacceptable, since the ratio K_p/K_s must approach asymptotically unity as χ approaches zero (or, as ϕ_t approaches ϕ_{max}) and suggests the existence of a non-linear relationship between K_p/K_s and χ.

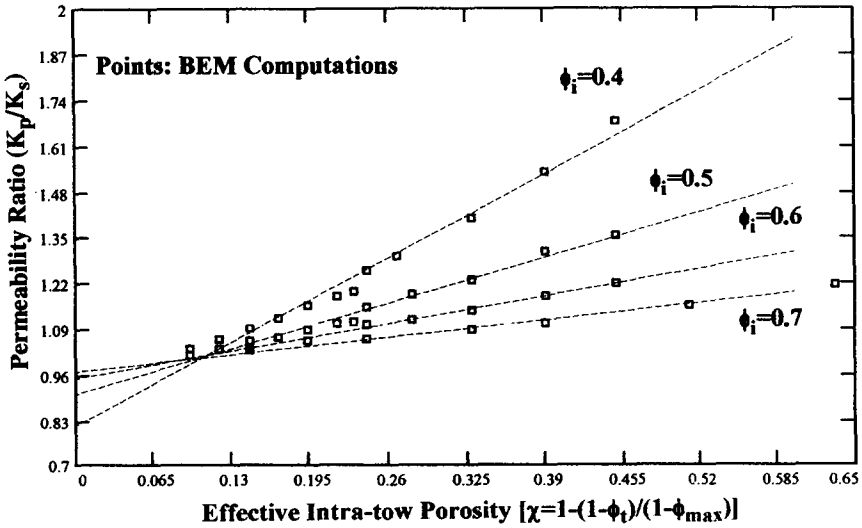

Figure 3. Permeability ratio K_p/K_s as function of the effective intra-tow porosity for four values of the inter-tow porosity ϕ_i. Also shown as broken lines are fitted linear functions of the form $(K_p/K_s) = A\chi + B$; $\chi = 1 - (1 - \phi_t)/(1 - \phi_{max})$.

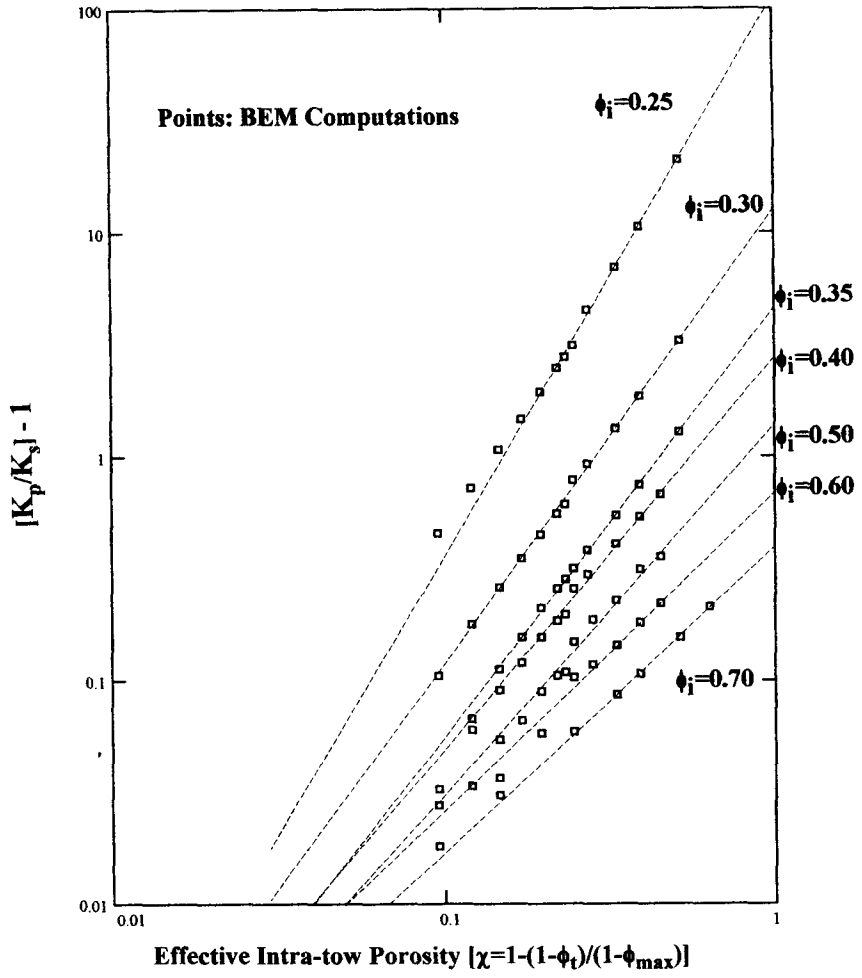

Figure 4. The variation of the quantity $(K_p/K_s - 1)$ with χ at various levels of the inter-tow porosity. Shown are also the fitted functions of the form of [9].

The BEM results can be better visualised in terms of an "intrinsic" permeability, defined as

$$K_{in} \equiv \frac{K_p}{K_s} - 1.$$

By plotting K_{in} against the effective intra-tow porosity χ as shown in figure 4, it becomes evident that a power-law relationship exists between $[(K_p/K_s) - 1]$ and (χ):

$$K_{in} \equiv \frac{K_p}{K_s} - 1 = \alpha(\phi_i) \cdot \chi^{\beta(\phi_i)} \qquad [9]$$

where the coefficients α and β are functions of the inter-tow porosity ϕ_i. Equation [9] exhibits the anticipated asymptotic behaviour as $\chi \to 0$ and is capable of representing the BEM results, with reasonable accuracy, for the entire range of ϕ_i and ϕ_t examined. The fitted functions of the form of [9] are also shown as broken lines in figure 4. Table 2 lists the least-squares values of the parameters α and β for the range of ϕ_i considered. It is evident that α is indeed a very strong function of the inter-tow porosity.

The results of table 2 for α can be represented well by functions of the form:

$$\alpha(\phi_i) = \frac{\lambda}{(\phi_i - \phi_m)^\delta} \quad \text{for } \phi_i > 1 - \pi/4 \qquad [10]$$

as can be seen in figure 5, where λ and δ are parameters to be determined. Best-fit estimates of

Table 2. Values of the parameters α and β [9] obtained from least-squares fitting of the BEM computational results, for various values of the inter-tow porosity ϕ_i

ϕ_i	α	β
0.25	112	2.49
0.30	12.7	2.03
0.35	4.63	1.92
0.40	2.78	1.75
0.50	1.39	1.65
0.60	0.689	1.42
0.70	0.396	1.37

λ and δ are shown in figure 5, along with the corresponding confidence intervals. Through [10], [9] can be written explicitly in terms of ϕ_i and ϕ_t as:

$$K_{in} \equiv \frac{K_p}{K_s} - 1 = \frac{\lambda}{(\phi_i - \phi_m)^\delta} \cdot \left[1 - \frac{1-\phi_t}{1-\phi_m}\right]^{\beta(\phi_i)} \qquad [11]$$

where K_s can be calculated from existing models (Bruschke and Avain 1993b; Gebart 1992), $\beta(\phi_i)$ can be found from table 2 and the values of λ and δ are shown in figure 5. Equation [11] derives from the computational results of the present study and comprises an empirical predictive model for the effective permeability of arrays of permeable fiber tows, in which the influence of the two porosities ϕ_i and ϕ_t is explicitly present. The model contains three parameters (λ, β and δ) whose values, for square packing of fibers, have been determined from the BEM results of the present study.

3.3. *A model for K_p in the range of low porosities*

It was pointed out by one of the reviewers that combinations of high values of ϕ_t with low values of ϕ_i are unrealistic in the field of composites manufacturing, since one cannot pack fiber tows without packing the fibers themselves. This is of course correct. We chose to present the results of our computations for the entire range of ϕ_i and ϕ_t examined in the previous section in order to give a more complete picture. Combinations of high ϕ_t with low ϕ_i can be encountered in other applications involving flow through arrays of fiber clusters, for example in hollow-fiber bioreactors, heat exchangers or flow of concrete through reinforcing steel preforms. In this section we

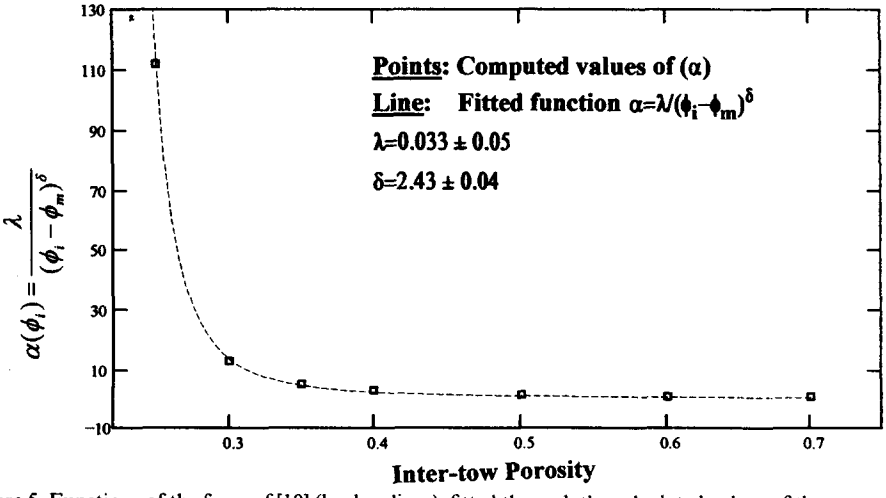

Figure 5. Functions of the form of [10] (broken lines), fitted through the calculated values of the parameter α (points) for the entire range of inter- and intra-tow porosities. The estimated values of the parameters λ and δ are also shown.

Table 3. Values of the parameters α and β [9] obtained from least-squares fitting of the BEM computational results at lower values of ϕ_i and ϕ_t

ϕ_i	α	β
0.25	61.3	2.11
0.30	15.9	2.17
0.35	5.76	2.05
0.40	4.24	2.03
0.50	2.58	2.07

concentrate on the interpretation of the BEM results at a range of inter- and intra-tow porosities more likely to be encountered in composites manufacturing, namely $\phi_i < 0.50$ and $\phi_t < 0.45$.

When [9] is fitted through the BEM results of figure 4 at the lower porosity end (by considering the points with $\phi_t < 0.4$ for $\phi_i = 0.25$ and the points with $\phi_t < 0.45$ for $\phi_i = \{0.3, 0.35, 0.4, 0.5\}$), the obtained power-law exponents are largely independent of ϕ_i as can be seen in table 3.

Furthermore, the values obtained for α can be fitted remarkably well to [10], as shown in figure 6. Table 3 and figure 6 suggests that the BEM results at these levels of porosity should collapse into a single curve, with power-law exponent around 2.1, if the quantity

$$\tilde{K} \equiv \left(\frac{K_p}{K_s} - 1\right) \cdot \frac{1}{\alpha} = \left(\frac{K_p}{K_s} - 1\right) \cdot \frac{(\phi_i - \phi_m)^{\delta}}{\lambda} \qquad [12]$$

is plotted against the effective intra-tow porosity χ. When the original computational results are transformed as suggested by [12], they do, to a reasonable degree, collapse on a single curve as shown in figure 7. This suggests that for the range of lower inter- and intra-tow porosities outlined previously, the permeability of a square assembly of permeable fiber tows (with square packing of the intra-tow filaments) can be expressed as a power-law function of χ:

$$\frac{K_p}{K_s} \cong 1 + \frac{\lambda}{(\phi_i - \phi_m)^{\delta}} \cdot \chi^{2.1} \quad \text{for} \quad \phi_t < 0.45 \text{ and } 0.25 < \phi_i < 0.5 \qquad [13]$$

with the values of λ and δ obtained from figure 6.

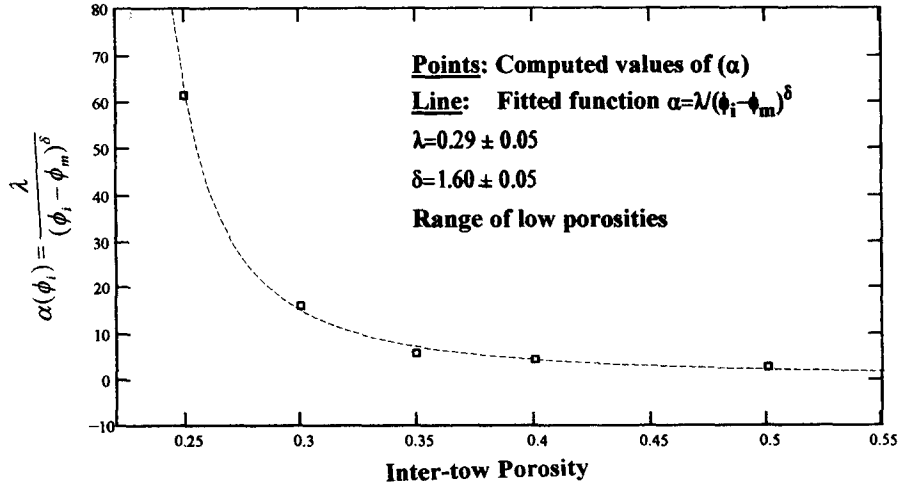

Figure 6. Functions of the form of [10] (broken lines), fitted through the calculated values of the parameter α (points) for the range of lower inter- and intra-tow porosities. The estimated values of the parameters λ and δ are also shown.

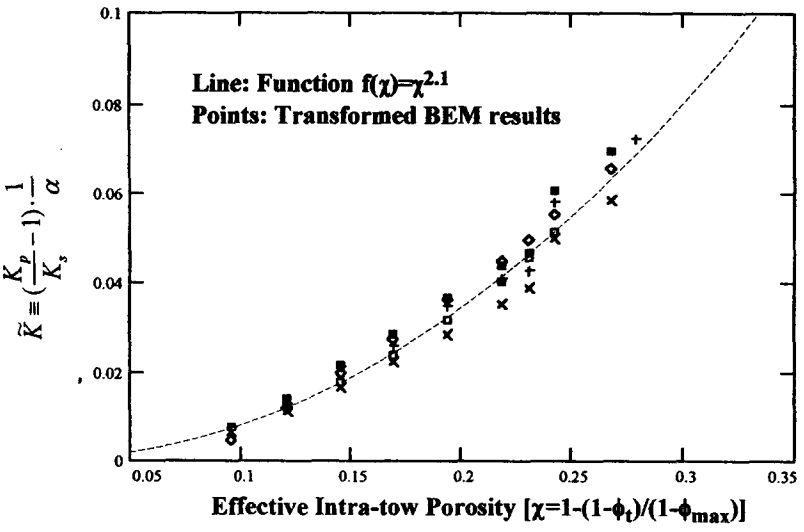

Figure 7. Variation of the transformed quantity.

$$\tilde{K} \equiv \left(\frac{K_p}{K_s} - 1\right) \cdot \frac{(\phi_i - \phi_m)^\delta}{\lambda}$$

with χ (λ and δ are from figure 6, obtained for lower values of inter- and intra-tow porosities) suggesting that the transformed data collapse onto the curve $f(\chi) = \chi^{2.1}$ (broken line). □: $\phi_i = 0.25$; ×: $\phi_i = 0.30$; ◇: $\phi_i = 0.35$; ■: $\phi_i = 0.40$; +: $\phi_i = 0.50$.

4. CONCLUSIONS

The interaction between inter- and intra-tow structure during Stokes flow across arrays of fiber tows aligned normal to the main direction of flow and its effect on the macroscopic permeability has been studied computationally using the method of boundary elements. A uniform square packing of fiber tows is considered, in which each unit cell consists of one tow containing a number of fiber-like filaments arranged again in square packing. Computer simulations for ϕ_i between 25 and 70% and ϕ_i between 30 and 60% suggest that a power-law relationship of the form:

$$\frac{K_p}{K_s} = 1 + \alpha\chi^\beta$$

where α and β are functions of ϕ_i, can describe the dependence of the effective permeability of the assembly on ϕ_t and ϕ_i. In the region of low inter- and intra-tow porosities (which is of practical significance in the field of composites manufacturing), a scaling is proposed according to which the computational results for K_p ($0.25 < \phi_i < 0.5$) collapse on a power-law curve with exponent 2.1 when plotted as suggested by [12] against the effective intra-tow porosity χ.

REFERENCES

Brebbia, C. A. and Dominguez, J. (1992) *Boundary Elements: An Introductory Course*, 2nd Edition. Computational Mechanics Publications, Southampton.

Bruschke, M. V. and Advani, S. G. (1993a) LIMS user's manual. Centre for Composite Materials, University of Delaware, Newark, Delaware.

Bruschke, M. V. and Advani, S. G. (1993b) Flow of generalised Newtonian fluids across a periodic array of cylinders. *J. Rheol.* **37**, 479–498.

Darcy, H. (1856) *Les Fonataines Publiques de la Ville de Dijon*. Dalmont, Paris.

Drummond, J. E. and Tahir, M. I. (1984) Laminar viscous flow through regular arrays of parallel solid cylinders. *Int. J. Multiphase Flow* **10**, 515–540.

Gebart, B. R. (1992) Permeability of unidirectional reinforcements for RTM. *J. Composite Materials* **26**, 1100–1133.

Gutowski, T. G., Cai, Z., Bauer, S., Boucher, D., Kingery, J. and Wineman, S. (1987) Consolidation experiments for laminate composites. *J. Composite Materials* **21,** 650–669.

Ingber, M. S. and Li, J. (1991) Surface pressure solution for BEM analysis of Stokes' flow. *Communications in Applied Numerical Methods* **7,** 367–376.

Ladyzhenskaya, O. A. (1963) *The Mathematical Theory of Viscous Incompressible Flow*. Gordon and Breach, New York.

Lam, R. C. and Kardos, J. L. (1991) The permeability and compressibility of aligned and cross-plied carbon fiber beds during processing of composites. *Polym. Eng. Sci.* **31,** 1064–1070.

Larson, R. E. and Higdon, J. J. L. (1986) Microscopic flow near the surface of two-dimensional porous media. Part 1. Axial flow. *J. Fluid Mech.* **166,** 449–472.

Larson, R. E. and Higdon, J. J. L. (1987) Microscopic flow near the surface of two-dimensional porous media. Part 2. Transverse flow. *J. Fluid Mech.* **178,** 119–136.

Lewis, T. B. and Nielsen, L. E. (1970) Dynamic mechanical properties of particulate-filled composites. *J. Appl. Pol. Sci.* **14,** 1449.

Lundstrom, T. S. and Gebart, B. R. (1995) Effect of perturbation of fiber architecture on permeability inside fiber tows. *J. Composite Materials* **29,** 424–443.

Nagelhout, D., Bhat, M. S., Heinrich, J. C. and Poirier, D. R. (1995) Permeability for flow normal to a sparse array of fibers. *Material Science and Engineering* **A191,** 203–208.

Papathanasiou, T. D. (1996) A structure-oriented micromechanical model for viscous flow through square arrays of fiber clusters. *Composites Science and Technology* (to appear).

Papathanasiou T. D., Ingber, M. S., Mondy, L. A. and Graham, A. L. (1994) The effective elastic modulus of fiber reinforced composites. *Journal of Composite Materials* **28,** 288–304.

Parnas, R. S. and Phelan, F. R. (1991) The effect of heterogeneous porous media on mold filling in resin transfer molding. *SAMPE Quart.* **22,** 53–60.

Phan-Thien, N., Tran-Cong, T. and Graham, A. L. (1991) Shear flow of periodic arrays of particle clusters: a boundary-element method. *J. Fluid Mech.* **228,** 275–293.

Phelan, F. R. and Wise, G. (1996) Analysis of transverse flow in aligned fibrous porous media. *Composites Part A* **27,** 25–34.

Pillai, K. M. and Advani, S. G. (1995) Numerical and analytical study to estimate the effect of two length scales upon the permeability of a fibrous porous medium. *Transport in Porous Media* **21,** 1–17.

Pillai, K. M., Luce, T. L., Bruschke, M. V., Parnas, R. S. and Advani, S. G. (1993) Modelling the heterogeneities present in preforms during mold filling in RTM, *25th International SAMPE Technical Conference*, Vol. 25, pp. 279–293.

Pozrikidis, C. (1992) *Boundary Integral and Singularity Methods for Linearised Viscous Flow*. Cambridge University Press, Cambridge.

Sadiq, T. A. K., Advani, S. G. and Parnas, R. S. (1995) Experimental investigation of transverse flow through aligned cylinders. *Int. J. Multiphase Flow* **21,** 755–774.

Sangani, A. S. and Acrivos, A. (1982) Slow flow past periodic arrays of cylinders with application to heat transfer. *Int. J. Multiphase Flow* **8,** 193–206.

Skartsis, L., Kardos, J. L. and Khomami, B. (1992) Resin flow through fiber beds during composite manufacturing processes. Part I: Review of Newtonian flow through fiber beds. *Polymer Engineering and Science* **32,** 221–230.

Summerscales, J. (1993) A model for the effect of fiber clustering on the flow rate in resin transfer moulding. *Composites Manufacturing* **4,** 27–31.